Fluid Phase Equilibria 572 (2023) 113834

Contents lists available at ScienceDirect

Fluid Phase Equilibria

journal homepage: www.journals.elsevier.com/fluid-phase-equilibria

What is the correct interfacial tension between methane and water at high-pressure/high-temperature conditions?

Bård J.A. Bjørkvik

SINTEF Industry, Applied Geoscience, Trondheim NO-7033, Norway

ARTICLE INFO

Keywords:
Interfacial tension
Methane
Water
Pendant drop
Standing bubble

ABSTRACT

The purpose of this communication is to draw attention to a puzzling inconsistency in the published data for the interfacial tension between methane and water at high-pressure and high-temperature conditions. The published data sets fall into two categories – those exhibiting linear dependence of interfacial tension on temperature, in agreement with the phenomenological Eötvös rule, and others exhibiting a peculiar and seemingly reproducible non-linear trend. The inconsistency seems to have gone largely unnoticed. That is somewhat disconcerting considering that the methane/water system is a commonly used reference system for evaluation of fluid interfacial tension models. The literature data are reviewed, discussed, and compared with a novel set of interfacial tension data for the methane/water system obtained in this study.

1. Introduction

During an experimental study of the interfacial tension (IFT) between a sample of natural retrograde gas (gas condensate) and formation water from a North Sea high-pressure/high-temperature (HP/HT) reservoir, we used the methane/water system as reference system for validation of the HP/HT reservoir-gas/brine IFT analysis. The methane/water system was selected because it is well-documented in the literature and because its characteristics are in many respects like those of the studied reservoir gas/brine system (excepting of course gas phase dewpoint as exhibited by the retrograde gas). When comparing our reference measurements with the literature methane/water IFT data, we made one unexpected observation that could be of general interest. The aim of this communication is to draw attention to that observation.

The methane/water system at elevated pressure and temperature has been studied by several independent research groups in recent years. In many cases that has been in the context of large-scale storage of carbon dioxide in nearly depleted gas fields. Liu et al. [1] present a comprehensive overview of experimental gas/water IFT data for methane, carbon dioxide and some other gases. We selected the methane/water system to validate our reservoir-gas/brine IFT analysis believing it to be a simple reference fluid system at HP/HT conditions. However, closer inspection of the literature data revealed a remarkable inconsistency between the published data sets that seems to have gone unnoticed. It has indeed been recognised by many workers over the last 30 years, e.g. [2–7], that there is surprisingly large variation (of the order of 10%) between literature data sets for the methane/water IFT at elevated pressure and temperature. For example, Sachs and Meyn [4] comment on "the extreme problems in achieving precise data for this system." The literature data indicate that there are probably components of uncertainty arising both from random and systematic effects. However, no one seems to have recognised that the published data sets seem to fall into two distinct categories, as will be demonstrated here. That is of concern because many recent modelling works of gas/water IFT at HP/HT conditions use the methane/water system for reference, e.g. [1,8-11]. Discrepancies of the order of 10% in the IFT may not seem dramatic, but it is puzzling considering the simple nature of the system and that it is one of the more thoroughly studied gas/water systems at elevated pressure and temperature. One could speculate whether the discrepancy observed for this specific fluid system calls for an explanation outside the inherent uncertainties of the experimental methods applied.

We review and discuss the relevant literature data in light of the new methane/water IFT data from our laboratory and offer some new perspectives on the mentioned inconsistency. The literature data are discussed on the background of a detailed analysis of the uncertainties of our IFT analysis. Although our methane/water IFT measurements in this work are of limited extent, they may nevertheless represent a useful addition to published data, considering that literature data on methane/water IFT at HP/HT conditions are still scarce.

In this work, IFT was measured by the axisymmetric drop shape analysis (ADSA) method [12]. The methane/water IFT was measured at two temperatures, 373.15 K and 448.45 K, in the pressure range

E-mail address: bard.bjorkvik@sintef.no.

https://doi.org/10.1016/j.fluid.2023.113834
Received 22 December 2022; Received in revised form 19 April 2023; Accepted 27 April 2023
Available online 1 May 2023

between approximately 10 MPa and 100 MPa. The measurement at 373.15 K gave opportunity for direct comparison with several literature data sets obtained for that temperature (or equivalently, 100 °C or 212°F). The measurement at 448.45 K corresponds to the reservoir temperature of the studied retrograde-gas reservoir. The reservoir-gas/brine IFT measurements and one further reference IFT data set obtained for methane and synthesised formation water at 448.45 K, representing the reservoir brine (16.0 wt% salts), are probably of more limited interest and will not be discussed here – only referred to when appropriate to establish the context of the methane/pure-water IFT reference measurements.

2. Materials and methods

2.1. Fluids

The water used for preparation of the methane/water system was reverse osmosis water (resistivity > 15 MΩ·cm) from an ELGA Purelab Option DV25 water purification system. The methane gas was industry grade gas of purity > 99.5% (AGA).

2.2. Experimental setup

The standing-bubble configuration of the ADSA method (gas bubble in water) was chosen instead of the complementary pendant drop configuration (water drop in gas). The standing-bubble configuration was chosen to minimise the volume of pressurised gas (both for safety reasons and because only a small sample of reservoir gas was available). A sketch of the experimental set-up is shown in Fig. 1. The measurement cell had two axially mounted sapphire windows with backlight illumination allowing full view of a radially mounted needle tip used to form standing bubbles of gas in the water phase. For technical information, see Table 1.

Table 1
Specifications of standing-bubble set-up.

Component	Comment
Standing-bubble/pendant-drop IFT measurement cell	In-house design (cell body Hastelloy C)
Cell windows	Sapphire windows 37 mm diameter, 15 mm thickness. Light opening 21 mm. Optical axis normal to polished surfaces to eliminate birefringence.
Maximum working pressure	200 MPa at 240 °C
Cell volume	45 cm^3
Needle tip diameter	In these measurements: external diameter (0.908 ± 0.001) mm, internal diameter (0.603 ± 0.001) mm
Wetted parts	Hastelloy C, sapphire, Teflon™, Viton™ and stainless steel (needle tip)
Pressure system	Hand-operated HIP pressure pumps
Pressure sensor	In these measurements: Paroscientific Digiquarz 420KR-HT-101 (20,000 psi range) calibrated with a Ruska dead weight tester. Accuracy ± 0.001 MPa.
Temperature sensor	RTD Pt100 calibrated with a secondary temperature standard (Jofra CTC-140A). Accuracy ± 0.05 K.
Heating system	Electrical. Temperature stability better than ± 0.05 K.
Light source	Telecentric back-light illuminator with adjustable LED spotlight – blue
Imaging system	Canon EOS 5D Mark II with Carl Zeiss 61 mm/0.1 Luminar objective and bellows. Ratio of the pixel size of the camera chip and the size of the imaged bubble typically smaller than $5{\cdot}10^{-4}$.
Drop shape analysis software	In-house software
Vibration insulation	Newport Vision IsoStation similar to standard item M-VIS3648-SG2–325A but with B Series Damping Isolation

2.3. Experimental procedures

The bubble shape is governed by the combined effect of IFT and gravity (buoyancy). It is described mathematically by the Young-Laplace equation, in terms of the ratio of the IFT and the water/gas density difference, e.g. [12]. This ratio was determined by matching a numerical integration of the Young-Laplace equation to the observed bubble shape by a full-contour bubble/drop shape analysis method adapted from Jennings Jr. and Pallas [13]. The IFT was calculated by multiplying the determined ratio with the density difference between water and gas.

Unambiguous determination of IFT for the methane/water system requires levels of surface-active impurities to be kept at an absolute

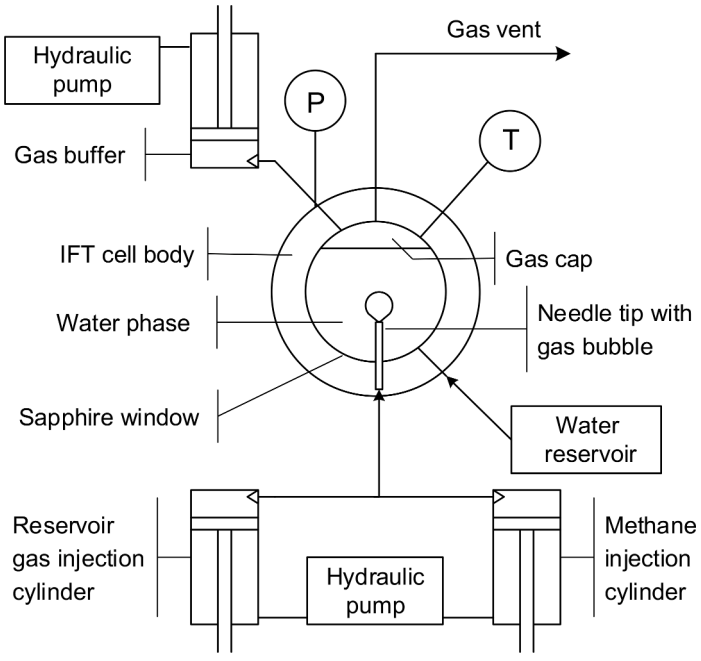

Fig. 1. Principle of standing bubble set-up for IFT measurement in reservoir-gas/brine and methane/water systems.

minimum. That was achieved by use of sufficiently pure methane and water and stringent procedures for cleaning and filling of the IFT measurement cell. Before measurement, the IFT cell was heated to approximately 60 °C and the sample chamber and connected flow lines were flushed with solvents (methanol for removal of water-soluble materials and toluene and hexane for removal of hydrocarbons). The sample chamber and connected tubing were then evacuated to a pressure below 10 Pa before the cell was filled with pure reverse osmosis water, pressurised with methane, and heated to approximately 175 °C overnight to eliminate possible microbial contamination. The cell was then emptied, cooled to 60 °C, and evacuated a second time before the water phase for the IFT analysis was drawn into the evacuated sample chamber. The cell was finally pressurised with methane and heated to target temperature.

The methane formed a gas cap of approximately 30% of the cell volume. The gas was injected from a 45 cm^3 piston cylinder (the methane injection cylinder in Fig. 1) or directly from a methane gas bottle by use of a gas booster. The methane bottle and the booster (not shown in Fig. 1) were also used to charge the methane injection cylinder and the buffer cylinder. The methane buffer cylinder was kept at constant temperature 60 °C, whereas the methane injection cylinder and the methane bottle/booster were at ambient temperature. Methane transferred to the needle tip of the IFT measurement cell was heated to cell temperature in the tubing inside the heated and insulated measurement cell set-up, immediately before the needle tip. The bubble formation was achieved by manipulating needle valves on the flowline.

Unambiguous determination of the IFT for the methane/water system relied on saturation of the water phase with methane before a methane bubble was introduced for measurement. Equilibration of the water phase with methane was in the present work achieved in the following way: During formation of the methane gas cap in the cell, methane was bubbled through the water phase. This served to reduce the time required for the water phase to equilibrate with the methane gas cap. Indications are that bubbling with methane also contributed to purging the water phase (by carrying surface-active trace impurities to the water/gas-cap interface). The pressure was adjusted to target pressure by use of the gas buffer cylinder (Fig. 1). During equilibration, small pressure adjustments were required as methane from the gas cap dissolved in the water phase. Stable pressure signalled that equilibrium had been reached. Equilibrium was verified also by observing the shape of test bubbles formed at intervals during the equilibration period. No further change in first-contact bubble shape confirmed that the water phase was fully equilibrated with the methane gas cap. Typically 2–3 h were required to reach equilibrium. However, the system was usually left overnight before measurements were started. Equilibrium was re-established by similar procedure after change in pressure and temperature conditions.

IFT measurements were taken on fresh gas bubbles. Several bubbles (at least 10) were released from the needle tip before forming a bubble for measurement to ensure that the gas had not been directly exposed to the water phase before the bubble was formed. Measurements were repeated for several fresh bubbles at each pressure stage – usually over a period of several days. The bubbles were monitored for varying length of time. By contrast to for example Kashefi et al. [14], the gas bubbles were formed in as short time as practical. Approximately 3–4 s was required to form a bubble (including time for attenuation of bubble vibrations). To determine the first-contact gas/water IFT value, a first bubble image was recorded as soon after formation as practical – typically within 5 s after the gas bubble emerged from the needle tip. However, the bubbles (typically 5–10) were monitored for a longer time period (up to 2–3 min) to ascertain the first-contact IFT value and to determine the equilibrium IFT value (if different from the first-contact IFT value). A smaller number of bubbles (typically 3–5) were monitored for an even longer time period (more than 20 min) to check for possible long-term IFT ageing effect.

A manually operated needle valve on the flow line was used to adjust the bubble volume to keep variations during measurement (because of temperature and pressure fluctuations) within narrow limits. The measurements were performed on bubbles sufficiently large to avoid problems with analysis sensitivity, but not so large as to enter into problems with bubble stability, e.g. [15–17].

Bubble volume sufficiently large to avoid problems with analysis sensitivity can be quantified by various non-dimensional numbers such as the classical Bond number, e.g. [15], the Worthington number introduced by Berry et al. [16], or the Neumann number introduced by Yang et al. [17]. For the standing bubble configuration, the Worthington number W_o is a convenient measure [16]:

$$W_o = \frac{\Delta\rho g V_b}{\pi\gamma d_n} \tag{1}$$

Here, $\Delta\rho$ is the density difference between the surrounding phase and the bubble, g is the gravitational acceleration, V_b is the bubble volume, γ is the IFT, and d_n is the needle diameter. The Worthington number scales from 0 to 1, where the larger values of W_o indicate the better measurement sensitivity. Berry et al. [16] have shown that W_o should be larger than approximately 0.6 for the standard deviation across a data set to be smaller than 1%. In the methane/water IFT measurements reported below, the bubble volume was typically $(7.0–8.5)\cdot10^{-3}$ cm^3 at 373.15 K and $(6.0–7.0)\cdot10^{-3}$ cm^3 at 448.45 K. The corresponding value of W_o, calculated by Eq. (1) with IFT and density values given in Table S1 in the supplementary material, ranges from approximately 0.61 to 0.79. The appropriate needle diameter used to estimate W_o by Eq. (1) is the inner diameter of 0.603 mm (cf. Table 1). That is because the gas bubble does not wet the needle tip and is therefore suspended from the inner circumference of the tip – not the outer (the methane bubbles behave like the nitrogen bubbles of the validation experiment, displayed in Fig. 2a).

However, the outer diameter of the needle tip (cf. Table 1) was used to calibrate the magnification factor of the images. That was done by relating the observed pixel dimensions of the needle tip to its metrical dimensions. As seen from Eq. (1), proper calibration is important because the IFT correlates with the ratio V_b/d_n, which scales as length squared.

2.4. Validation experiment

The IFT analysis procedure was validated by measurement of the surface tension of pure water at 298.15 K (± 0.10 K) and atmospheric pressure. The surface tension was determined from bubbles of nitrogen gas formed in water. Approximately 200 measurements were obtained for bubbles of varying sizes. Fig 2a shows five example bubbles of different Worthington number. Fig. 2b presents the calculated IFT values for all bubbles as function of Worthington number.

Except for use of nitrogen gas instead of methane and lower temperature and pressure, the experimental set-up and data analysis procedure were identical to those used for the methane/water IFT analysis. The density values of nitrogen and pure water required for the analysis were taken from the NIST REFPROP data base [19].

Fig. 2b shows that the spread of the data points decreases with increasing Worthington number. That is, the sensitivity of the IFT analysis increases with Worthington number, in agreement with the results presented by Berry et al. [16]. We obtained these 200 reference measurements by allowing a constant stream of nitrogen bubbles to form at the needle tip. The bubble images were obtained in a random manner, representing all stages of bubble growth from that of small bubbles immediately after they emerged from the needle tip to large bubbles just before they detached from the needle tip. The gas feed rate and hence, the bubble growth rate, was approximately the same for all bubbles. The growth rate was such that the bubbles detached from the needle tip after approximately 20 s. Because bubbles were formed at constant growth rate, the calculated value of W_o was for each bubble approximately proportional to the bubble age. The bubble age can be read on the secondary horizontal axis in Fig. 2b.

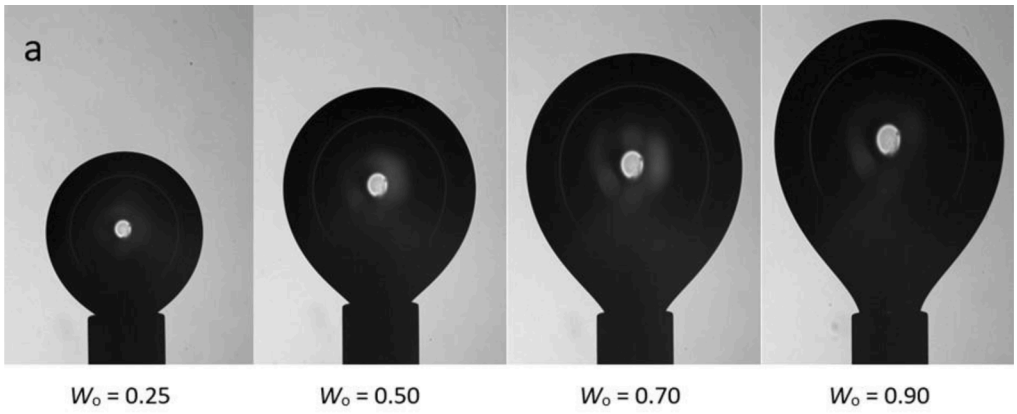

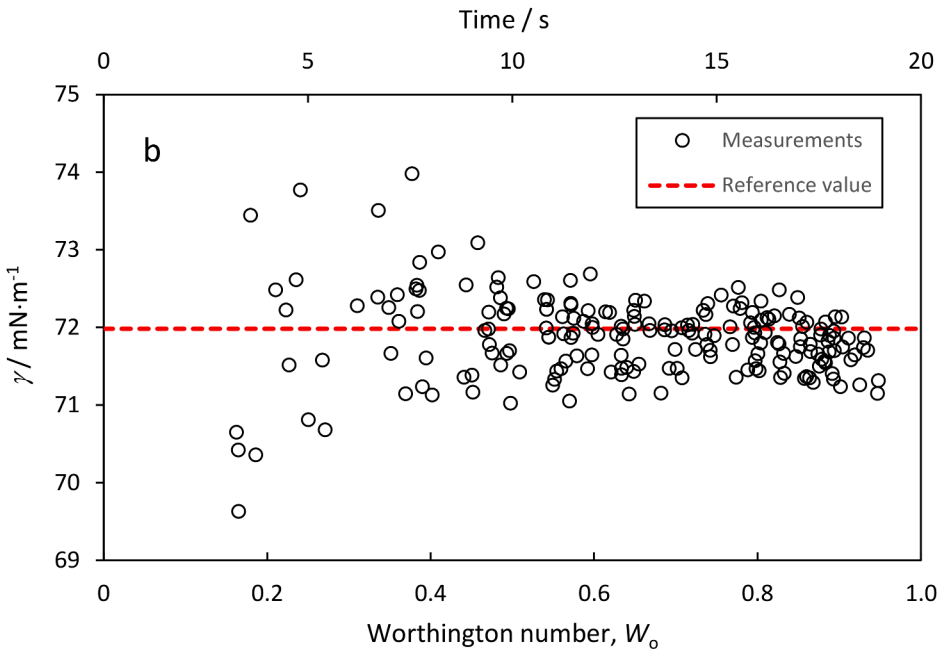

Fig. 2. (a) Example bubbles of nitrogen in pure water at 298.15 K and atmospheric pressure illustrating change of size and shape with increasing Worthington number, W_o. (b) ADSA measurements of surface tension of pure water at 298.15 K and atmospheric pressure versus Worthington number, W_o. Because bubbles were formed at constant growth rate (see adjoining text below for details), the calculated value of W_o was for each bubble approximately proportional to the bubble age. The bubble age is indicated on the secondary horizontal axis. The dashed line indicates the recommended reference surface tension value of water, 71.98 mN·m^{-1} [18].

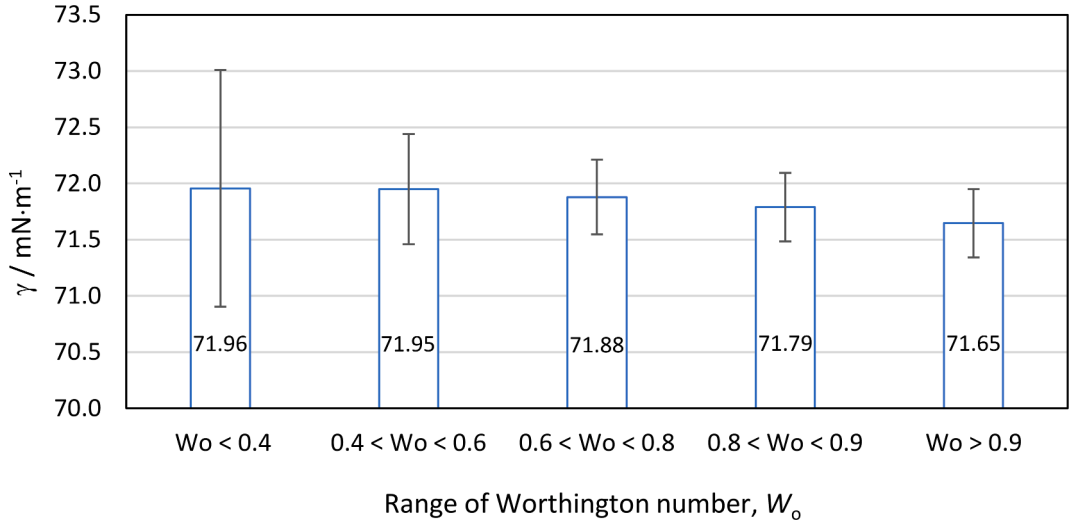

Fig. 3. Histogram showing average IFT values calculated for five different ranges of Worthington number, W_o, in Fig. 2b. The standard deviation is indicated by error bars. The recommended reference surface tension value of water is 71.98 mN·m^{-1} [18].

It is noted in Fig. 2b that the IFT values seem to decrease slightly with increasing W_o. That is probably not caused by any systematic error in the data analysis but reflects adsorption of trace impurities at the nitrogen/water interface. As indicated in Fig. 2b, the larger bubbles required longer time to form than the smaller bubbles and they were therefore more susceptible to IFT decrease by diffusion of trace impurities from the water phase to the interface. This illustrates the challenge involved in measuring accurately the surface tension of pure water. However, as shown in Fig. 3, the effect of trace impurities was relatively small.

The histogram in Fig. 3 presents the calculated average IFT value of the data points in Fig. 2b for five ranges in W_o. The standard deviation is indicated by error bars. Even for the larger bubbles ($W_o > 0.9$), which are assumed to be most affected by surface active trace impurities, the average IFT value agrees with the recommended reference value 71.98 mN·m^{-1} [18] within approximately one standard deviation (0.30 mN·m^{-1}). It is also noted that the recommended reference value is given with an uncertainty of 0.36 mN·m^{-1} [18].

Fig. 3 shows that the average IFT value for $W_o < 0.6$ is close to the literature value of 71.98 mN·m^{-1}, indicating that the analysis was not influenced by significant systematic errors. This observation lends confidence to the magnification factor employed in the bubble image analysis. However, the analysis sensitivity for the smaller bubbles is rather poor, and the standard deviation of the measurements relatively large. For the larger bubbles ($W_o > 0.6$) the standard deviation decreases to approximately 0.3 mN·m^{-1}, corresponding to relative uncertainty approximately 0.4%. This appears to be the non-reducible uncertainty level of our image analysis. However, it is noted that the analysis was intended to be representative of everyday practice in the laboratory. It could possibly be optimised to yield somewhat lower repeatability uncertainty.

With that said, there are some inherent sources of variability in the analysis that cannot be eliminated entirely. For example, even with superb vibration isolation of the measurement cell, the bubble could be subject to small vibrations set up by temperature induced convection currents in the bulk phase of the cell. Also, the bubble represents an obstacle to the parallel light beam used to illuminate and image the bubble, which results in Fresnel diffraction at the imaged contour of the bubble. The more monochrome illumination, the sharper the diffraction bands. However, the effect cannot be eliminated by broadening the wavelength spectrum of the light source. That will only cause smearing out of the diffraction pattern and make the contour less sharp. This effect could represent a source of systematic error in the contour detection algorithm, but because the parameters of the algorithm are usually varied somewhat from one image to another, the effect is probably predominantly random. In any case, the effect is relatively small. The typical width of the Fresnel diffraction pattern is small (of the order of microns) compared to the bubble dimensions (of the order of millimetres). The same type of Fresnel diffraction pattern can be observed also at the imaged contour of the needle tip where it may introduce a slightly larger uncertainty in the analysis. That is because the width of the needle tip relative to that of the diffraction pattern is smaller than for the bubble and because determination of the pixel dimensions of the needle tip is crucial for correct calibration of the image magnification.

2.5. Uncertainty analysis

The relative combined standard uncertainty of the IFT analysis is estimated to be approximately 0.7%. This estimate is based on the law of propagation of uncertainty [20]. First, it is required to consider the uncertainty of the experimental temperature and pressure. It will be recognised that the interfacial tension for a binary system with two phases such as the methane/water system is uniquely determined by two independent thermodynamic variables, here taken as temperature and pressure (cf. the Gibbs phase rule, e.g. [21]). Further, Eq. (1) implies that the uncertainty of the calculated IFT value depends explicitly on the uncertainty of additional quantities such as the density difference $\Delta\rho$ employed in the calculation and on the geometrical quantities of the bubble shape analysis, here represented by the ratio V_b/d_n and W_o. However, to determine the combined uncertainty of the IFT value, it is required to consider also other sources of variability, such as the process related effects of impurities and system equilibration. Assuming that possible covariance associated with the various sources of variability can be ignored, we will estimate the relative combined standard uncertainty $u_{c,r}$ by the following expression for propagation of uncertainty:

$$u_{c,r}^2 = \left[\frac{1}{\gamma}\left(\frac{\partial\gamma}{\partial T}\right)u(T)\right]^2 + \left[\frac{1}{\gamma}\left(\frac{\partial\gamma}{\partial p}\right)u(p)\right]^2 + \left[\frac{u(\Delta\rho)}{\Delta\rho}\right]^2 + \left[\frac{2u(d_n)}{d_n}\right]^2 + \sum_i \left[\frac{1}{\gamma}\left(\frac{\partial\gamma}{\partial x_i}\right)u(x_i)\right]^2 \quad (2)$$

In the first and second term on the right side of Eq. (2), $u(T)$ and $u(p)$ are the standard uncertainty of the temperature and pressure, respectively. In the third term, $u(\Delta\rho)$ is the standard uncertainty of the estimated density difference between the phases. In the fourth term, $u(d_n)$ is the standard uncertainty of the measured diameter of the needle tip. As mentioned above, that measure is critical because the imaged needle tip diameter is used to transform the pixel dimensions of the images to metric dimensions. In that transformation, the ratio V_b/d_n in Eq. (1) scales approximately as d_n^2, which explains the factor of 2 in the fourth term of Eq. (2). The summation term on the right side of Eq. (2) represents in symbolic form process related sources of variability (x_i) more difficult to quantify, such as technicalities of the bubble shape analysis, effects of impurities and fluid equilibration – and possibly also unknown sources of variability.

The partial derivatives in Eq. (2) are sensitivity coefficients. The partial derivatives of the IFT with respect to temperature and pressure are estimated from the experimental data in Fig. 5. We approximate the summation term on the right side of Eq. (2) by the relative repeatability uncertainty of the IFT squared, $\sigma_r^2(\gamma)$ (for numerical values of $\sigma(\gamma)$ and $\sigma_r(\gamma)$, see Table S1 in the supplementary material):

$$\sum_i \left[\frac{1}{\gamma}\left(\frac{\partial\gamma}{\partial x_i}\right)u(x_i)\right]^2 \sim \left[\frac{\sigma(\gamma)}{\gamma}\right]^2 = \sigma_r^2(\gamma) \quad (3)$$

We substitute Eq. (3) into Eq. (2) and discuss the magnitude of the various terms of Eq. (2) under the following five headings: Uncertainty of (1) temperature, (2) pressure, (3) density difference, (4) needle diameter, and (5) the repeatability uncertainty of the IFT.

2.5.1. Uncertainty of temperature

With reference to the experimental IFT data in Fig. 5, the sensitivity coefficient ($\partial\gamma/\partial T$) in the first term on the right side of Eq. (2) is negative. The absolute value of the sensitivity coefficient, $|(\partial\gamma/\partial T)|$, decreases from approximately 0.16 mN·m^{-1}/K at 10 MPa to approximately 0.13 mN·m^{-1}/K at 100 MPa. For simplicity we ascribe the largest sensitivity value, 0.16 mN·m^{-1}/K, to all the data points. The temperature term in Eq. (2) takes a maximum value of approximately $(2.5{\cdot}10^{-4})^2$ at the higher pressures of the 448.45 K data set. For simplicity, we ascribe that value to all the data points. It is noted that the calculation is performed with $u(T) = 0.05$ K, corresponding to the uncertainty of the calibrated temperature probe (cf. Table 1). The standard uncertainty $u(T)$ does not include the effect of temperature fluctuations. Such fluctuations in the experiments are accounted for by the repeatability uncertainty of the IFT discussed below (Section 2.5.5).

2.5.2. Uncertainty of pressure

With reference to the experimental IFT data in Fig. 5, the sensitivity coefficient ($\partial\gamma/\partial p$) in the second term on the right side of Eq. (2) is negative over the experimental pressure range and takes its largest negative value approximately −0.4 mN·m^{-1}/MPa at 10 MPa. The pressure term in Eq. (2) takes the maximum value of approximately $(9{\cdot}10^{-6})^2$, which is much smaller than the temperature term. For

simplicity, we ascribe that value to all the data points. It is noted that the calculation is performed with $u(p) = 0.001$ MPa, corresponding to the uncertainty of the calibrated pressure sensor (cf. Table 1). The pressure fluctuations during measurements were significantly larger, but that effect is accounted for by the repeatability uncertainty of the IFT discussed below (Section 2.5.5).

2.5.3. Uncertainty of density difference

We use the density difference between the mutually saturated phases of water and methane to calculate the IFT (cf. Section 2.3). The effect of methane saturation on pure water density and water saturation on pure methane density is small. The effect is within the uncertainty of most previously published measurements of the methane/water IFT and has often been assumed insignificant, e.g. [14,22,23]. However, the effect increases with increasing temperature and pressure.

For pure water at 373.15 K the effect of methane saturation on the water density is to decrease the density by approximately 0.7% at 100 MPa. The maximum error introduced in the IFT analysis by use of non-saturated water density is slightly larger (1.0%) because it is the density difference between water and methane that enters the calculation. At 448.45 K and 100 MPa we estimate the density of methane-saturated water to be approximately 1.3% smaller than that of non-saturated water, which causes a systematic error of 1.9% in the IFT analysis using non-saturated water density. That is a significant error compared to other uncertainties in the IFT analysis. To reduce the uncertainty of the IFT analysis, we therefore use density values of methane-saturated water as calculated by the modified Spivey–McCain, Jr.–North correlations [24]. These density estimates are assumed to be accurate within approximately 0.1%.

Because the density of methane is much smaller than that of water, the accuracy of the density difference is less sensitive to the accuracy of the methane density. The density of water-saturated methane has therefore in nearly all previous works like ours been approximated by the density of pure methane, as given for example by the NIST REFPROP data base [19]. We estimate that the error introduced in the IFT by using the density of water-free methane is smaller than 0.1% in the pressure range 10–100 MPa at 373.15 K but increases to 0.5% at the higher pressures at 448.45 K. The latter error approaches the level of other uncertainties in the analysis. For that reason, we have also accounted for the effect of water vapour on the density of methane. That was achieved in the following way: The above estimates of the error introduced by using the density of pure methane instead of water-saturated methane were obtained by use of a commercial fluid PVT simulation tool, PVTsim Nova 5 (Calsep), using the SRK-Peneloux equation of state. We believe the error estimates to be quite accurate because PVTsim gives density values for water-free methane that differ not more than 2% from the NIST data in the pressure range 10–100 MPa and yields water concentration of saturated methane that differ by not more than 5% from experimental data published by Yarrison et al. [25]. However, instead of directly applying the density data for water-saturated methane as obtained by PVTsim, an improved density estimate was obtained by multiplying the NIST data for pure methane by a scaling function obtained by use of PVTsim. The scaling function was determined by the ratio of the densities of water-saturated and water-free methane obtained by PVTsim.

We estimate that the uncertainty of the density difference is reduced to approximately 0.2% by use of the modified Spivey–McCain, Jr.–North correlations and the NIST data scaled by the function obtained by use of PVTsim. The density difference term in Eq. (2) is therefore $(2.0{\cdot}10^{-3})^2$ and hence, dominates the pressure and temperature terms.

2.5.4. Uncertainty of needle diameter

The standard uncertainty of the outer needle diameter, 0.908 mm (cf. Table 1), is 0.001 mm. The relative standard uncertainty is $1.1{\cdot}10^{-3}$ and the fourth term on the right side of Eq. (2) is $(2.2{\cdot}10^{-3})^2$. This term is therefore of the same magnitude as the density difference term.

2.5.5. Repeatability uncertainty of the IFT

The standard deviation obtained under repeatability conditions for each data point in Fig. 5 is given in Table S1 in the supplementary material. Table S1 also includes the calculated relative repeatability uncertainty. Apart from two data points that have relative repeatability uncertainty as large as approximately 1.5%, the other 23 data points out of the total 25, have relative repeatability uncertainty smaller than 0.6% (corresponding to approximately 0.3 mN·m^{-1}). For simplicity, we take that value to represent all the data points and calculate the fifth term on the right side of Eq. (2) as $(6{\cdot}10^{-3})^2$. We see that this term dominates the other terms of the equation. In the following we discuss the more important sources of variability encompassed by the repeatability uncertainty term under the following headings: (1) temperature and pressure stability, (2) impurities, (3) fluid equilibration, and (4) bubble contour analysis.

2.5.5.1. Temperature and pressure stability. Good temperature and pressure stability is necessary for proper fluid equilibration. The temperature and pressure stability of our measurements were to some extent connected. When gas was not transferred to the measurement cell, both short-term and long-term temperature stability was within ± 0.05 K. During injection of gas and formation of bubbles for measurement, short-term temperature variations (time scale minutes) were slightly larger because of pressure fluctuations associated with formation and volume-adjustment of the bubbles. The temperature stability during a measurement series at specified pressure was typically within ± 0.15 K. With reference to the value of the sensitivity coefficient ($\partial\gamma/\partial T$) discussed in Section 2.5.1, such temperature variation is not expected to give rise to IFT variation larger than approximately ± 0.02 mN·m^{-1}. The contribution of this source of variability to the overall repeatability uncertainty of ± 0.3 mN·m^{-1} is therefore relatively small. Neither are such short-term temperature fluctuations expected to cause significant change in water density by variation in gas saturation. As already noted, equilibration of the water phase was a relatively slow process (time scale hours) compared to the temperature fluctuations referred to (time scale minutes).

The short-term pressure stability (time scale minutes) was typically better than ± 0.03 MPa. With reference to the maximum (absolute) value of the sensitivity coefficient ($\partial\gamma/\partial p$) discussed in Section 2.5.2, such pressure variation is not expected to give rise to IFT variation larger than ± 0.01 mN·m^{-1}. The contribution of this source of variability to the overall repeatability uncertainty is therefore even smaller than that of the temperature fluctuations. However, pressure variations on a longer time scale than minutes could be significantly larger than ± 0.03 MPa, especially in the high-pressure range. The pressure variations for different bubbles formed over time could be ± 0.3% of the experimental target pressure. That is, the pressure variation at 100 MPa could be as large as ± 0.3 MPa. However, the larger pressure variations in the high-pressure range did not introduce any significant additional uncertainty in the IFT analysis. That is partly because the sensitivity coefficient ($\partial\gamma/\partial p$) approaches zero in the high-pressure range (cf. Fig. 5) and partly because re-equilibration of the water phase was a relatively slow process, which served to damp out the effect of pressure variations.

2.5.5.2. Impurities. Surface-active impurities cause the IFT of a freshly created gas/water interface to decrease. It was observed that fresh bubbles of methane formed in methane-saturated water revealed only very small decrease in IFT, typically less than 0.3 mN·m^{-1}. That is qualitatively in good agreement with the observations in the validation experiment discussed in Section 2.4. Such small decrease in IFT (which typically took place over the first 2–3 min) appeared random. Some bubbles displayed a small IFT decrease – others did not. This observation allows the following two conclusions:

- The apparently random IFT ageing effect observed for different bubbles suggests varying effect of water-borne surface-active trace impurities. This conclusion is strengthened in that bubbling of the water phase with methane before measurements appeared to reduce the IFT ageing effect (cf. Section 2.3).
- The barely significant ageing effect demonstrates very low levels of water-borne trace impurities. This conclusion is strengthened by the fact that the employed standing bubble configuration is extremely sensitive to such impurities. The small surface area of the gas bubble (0.1–0.2 cm^2) against the relatively large volume of water (in these measurements about 30 cm^3) makes the analysis very sensitive to water-borne impurities. For that reason, the standing bubble configuration is experimentally more challenging than the complementary pendant drop configuration.

The ageing effect on the IFT by trace impurities was reduced as far as possible by forming and imaging the bubbles in as short time as practical (approximately 5 s, cf. Section 2.3). From the observations in the validation experiment (Fig. 2 and Fig. 3), we do not expect bubbles formed within approximately 5 s to be significantly influenced by water-born trace impurities.

2.5.5.3. Fluid equilibration. Previously published data sets for the methane/water IFT indicate that proper system equilibration is a critical (perhaps *the* critical) factor in obtaining reliable IFT results at HP/HT conditions. As demonstrated by Hebach et al. [26] in an experimental study of the IFT between CO_2 and water, correct IFT can be determined for a gas/water system before mutual saturation of the phases is established, but that analysis requires use of the instantaneous densities of the undersaturated phases, which are usually not well-characterised. In practice, it is therefore more convenient to allow the phases to come to full equilibrium before measurement and then use the mutually saturated phase densities in the calculation of the IFT. We find that it is particularly important to pay attention to equilibration of the water phase using the standing bubble configuration because of the relatively large water phase volume, which makes the equilibration process slow. We believe that the experimental procedures described in Section 2.3 ensured full equilibration of the water phase with methane before measurements were taken, and therefore that equilibration effects did not contribute significantly to the repeatability uncertainty of the IFT.

Whereas the equilibration time for the water phase was typically of the order of hours, saturation of fresh bubbles of methane with water vapour is probably a rapid process – at least at the high temperatures of the present work. We were not able to observe any significant and repeatable change in IFT with time for fresh bubbles formed after the water phase had been equilibrated with methane. That indicates that saturation of the methane bubble by water vapour did not cause any significant change in IFT in our measurements or that the change took place before the first bubble image could be recorded – or both. Equilibration transients faster than 5 s (age of drop at first image) could not be detected with the present set-up.

It is noted that equilibration of reservoir-gas bubbles in brine above the dew-point pressure of the dehydrated reservoir gas (40.7 MPa) provided visual evidence for the rapid equilibration with water vapour. It was observed that the stability of the dehydrated reservoir gas broke down almost instantaneously when brought into contact with brine. This is illustrated in Fig. 4, showing a bubble of reservoir gas in brine at pressure approximately 1 MPa above the dewpoint pressure of the dehydrated gas (40.7 MPa). Images 4a, 4b, and 4c were taken after 5 s, 1 min, and 2 min, respectively. The noticeable elongation of the bubble with time signals IFT decrease, probably caused by diffusion to the gas/water interface of surface-active compounds carried by the reservoir gas.

Because of the different refractive indices of bubble and surrounding fluid, the beam of light passing through the bubble is refracted out of the optical path, causing the bubble to appear dark except in the central part where light is transmitted without significant refraction. It is therefore possible to view the interior of the bubble in that part. It is seen that droplets (in the micron range) formed almost instantaneously (within 5 s) inside the gas bubble upon contact with brine. These droplets segregated with time, but not very fast, which indicates that the density of the droplets was not very much larger than that of the gas. This suggests that the droplets consisted of heavy-end hydrocarbons. Probably, saturation of the gas by water vapour caused precipitation of heavier hydrocarbons, in effect increasing the dewpoint pressure from that of the dehydrated reservoir gas. Such increase of dewpoint pressure by water vapour is well-documented in the literature, e.g. [27]. (In this case the dewpoint pressure of the reservoir gas equilibrated with reservoir brine was increased by approximately 18 MPa relative to that of the dehydrated gas.)

2.5.5.4. Bubble contour analysis. Components of uncertainty of the image analysis can in principle arise from both random and systematic effects. However, the validation experiment described in Section 2.4 indicates that possible systematic effects were of little significance. We

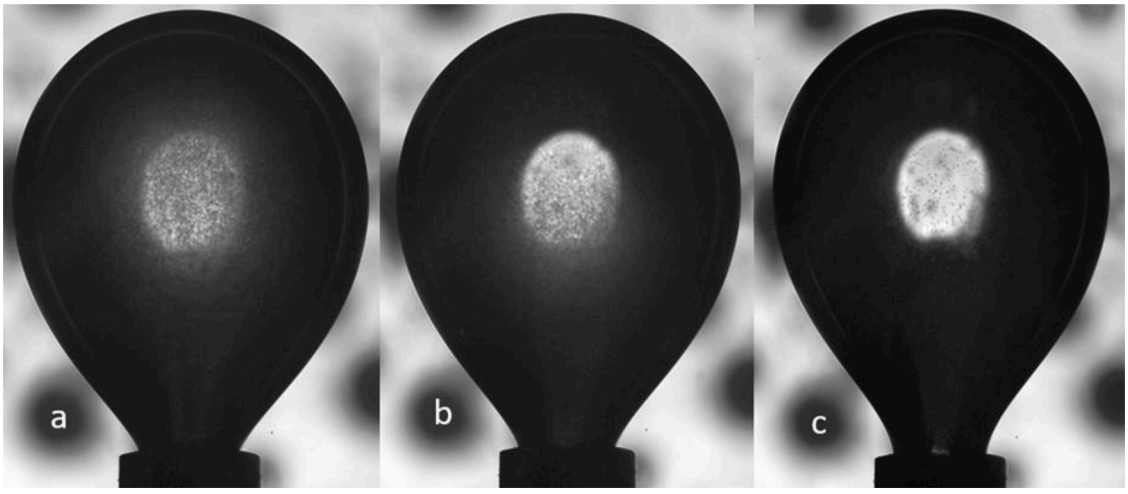

Fig. 4. Reservoir-gas bubble at 41.8 MPa and 448.45 K imaged at bubble age (a) 5 s, (b) 1 min, and (c) 2 min. The bubble dimensions can be inferred from the needle tip, which outer diameter is approximately 0.9 mm (cf. Table 1). Because light is refracted at the methane/water interface, the gas bubble appears opaque except in the central part where light is transmitted without significant refraction. In this central part of the drop, it is therefore possible to view the interior. (The diffuse dark spots around the bubble are out-of-focus tiny gas bubbles attached to the front cell window.).

believe that to be the case also for the methane/water IFT measurements and that predominantly random effects of the bubble contour detection dominate the repeatability uncertainty of the IFT. As shown by the validation experiment, the relative repeatability uncertainty for bubbles with Worthington number larger than 0.6 appeared to be approximately 0.4%. As stated above, the relative repeatability uncertainty of the methane/water IFT measurements appears to be somewhat larger, approximately 0.6% for methane bubbles with Worthington number in the range from 0.61 to 0.79 (cf. Section 2.3). We believe the additional uncertainty of the methane/water IFT analysis to be caused mainly by an optical distortion effect not present in the nitrogen/water IFT reference analysis – that caused by tiny gas bubbles attached to the cell windows. Although precautions were taken in design and heat insulation of the cell windows, it was not possible to avoid that the window surfaces had slightly lower temperature than the cell body. Under certain pressure and temperature conditions, the slightly lower surface temperature of the windows caused gas dissolved in the water phase to nucleate and form tiny gas bubbles attached to the windows (like those seen in Fig. 4). That is because the saturation level of methane in water decreases with decreasing temperature. Although such tiny gas bubbles at the front window were out of focus in images of the gas bubble standing at the needle tip, they sometimes caused smudging of the observed contour of the bubble at the needle tip. Fortunately, in most cases only parts of the drop contour were affected, and those parts could be omitted in the contour detection algorithm. However, that involved some variation in the number and distribution of edge pixels in the contour analysis and some variation in the parameters of the contour recognition algorithm. We believe such effects can explain the slightly larger relative repeatability uncertainty of the methane/water IFT analysis.

3. Results

Considering that the IFT observed for the methane/water system exhibited only minor and random ageing effects, only the first-contact IFT values are reported. Fig. 5 presents average IFT values obtained at 373.15 K and 448.45 K. Tabulated values of the IFT data points in Fig. 5 are given in Table S1 in the supplementary material.

The data were obtained by first measuring IFT for increasing pressures up to approximately 100 MPa and then for decreasing pressures down to approximately 10 MPa. This was done to verify that there was no long-term drift in the measured values. Measurements were first taken at 373.15 K, then at 448.45 K. The cell was emptied after measurements at 373.15 K and recharged with a sample of fresh water before measurements at 448.45 K. The main effect of increasing the temperature of the methane/water system from 373.15 K to 448.45 K was to shift the 448.45 K curve downwards approximately 24% without significant change in pressure dependence. Each data point in Fig. 5 represents the average value obtained for several (typically 5–10) individually formed methane bubbles. The relative repeatability uncertainty of the IFT was typically smaller than 0.6% (cf. Table S1). That uncertainty is smaller than the plotted symbols for the average IFT values in Fig 5. The typical pressure variation of the averaged data points in Fig. 5 was 0.3% of the experimental pressure (cf. Section 2.5.5.1). That variation is also smaller than the plotted symbols in Fig. 5.

The IFT trendlines in Fig. 5, valid in the pressure range 10–100 MPa, are of the form:

$$\gamma = A\exp\left(-\frac{p-B}{C}\right) + D \tag{4}$$

where *A, B, C*, and *D* are constants with numerical values given in Table 2.

4. Discussion

It is noted that the constant *D* in Table 2 represents the asymptotic IFT value in the high-pressure limit. This estimate might not be valid at pressures higher than 100 MPa. Experimental IFT data for the methane/water system presented by Wiegand [22] and Wiegand and Franck [23] indicate that the decreasing IFT trend with pressure is reversed for pressures above approximately 120 MPa at 373 K and 100 MPa at 473 K. The water and methane density values used in their analysis were not corrected for mutual solubility effects, though. Hence, the increasing trend in their IFT data at high pressures could be slightly overestimated. Nevertheless, such reversal of IFT decrease at high pressure is expected from recent fluid modelling works (based on density gradient theory and molecular dynamics simulation), e.g. [5,14,28,29].

Table 2
Parameters of fit for trendline of IFT between methane and water versus pressure, cf. Eq. (4), at temperature $T = 373.15$ K and 448.45 K.

Parameter	IFT trendline, cf. Eq. (4) $T = 373.15$ K	$T = 448.45$ K
A (mN·m^{-1})	13.26	10.45
B (MPa)	3.10	3.24
C (MPa)	24.35	22.60
D (mN·m^{-1})	40.91	31.19
St.dev. of fit (mN·m^{-1})	0.17	0.12

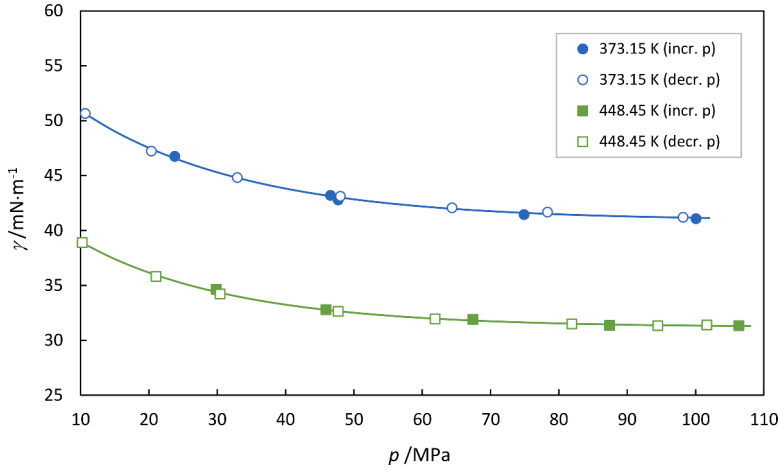

Fig. 5. Measured IFT, γ, between methane and water as function of pressure, p, at temperature 373.15 K and 448.45 K. Filled symbols represent data points obtained for increase in pressure, open symbols represent data points obtained for subsequent decrease in pressure. For each temperature, the data points (including both increasing and decreasing pressure) are fitted by a single trendline of form given by Eq. (4) with parameters of fit given in Table 2.

Our data at 373.15 K can be compared directly with several data sets in the literature. These data sets, which all of them were obtained by the ADSA method (pendant drop or standing bubble) are referred to in Table 3. Our data are compared with these literature data in Fig. 6.

It is noted that Table 3 is not intended to give an exhaustive overview of all IFT data in the literature for the methane/water system at 373 K – only such data sets that cover the whole or a large part of the pressure range investigated in this work ($p > 10$ MPa). For an overview of literature data restricted to lower pressures (< 10 MPa), see Reference [1]. It is also noted that Table 3 does not include an older data set of Hough et al. [33], which covers the whole pressure range investigated in this work. As pointed out by Jennings and Newman [30], that data set is probably biased by impurities at temperatures higher than room temperature (possibly from organic sealing materials of the measurement cell).

Comparison of the data sets in Fig. 6 shows that our data fall well within the range of previously published data sets and are seen to be in excellent agreement with the recent data set of Kashefi et al. [14]. Excepting the data of Shariat [32] at the lower pressures, the data of Wiegand [22], Sachs and Meyn [3], and Tian et al. [31] represent the upper bound to the range of the data. The deviation between the latter three data sets appears to be small. The lower bound to the range of the data is represented by the data of Jennings and Newman [30].

In Fig. 6, it is seen that the data of Shariat [32] appear anomalously high at the lower pressures, as commented also by Zhang et al. [34]. The extrapolation of the data to the low-pressure limit is clearly not consistent with the expected IFT, which should approach the surface tension of water, given as 58.92 mN·m^{-1} [18]. The reason for the discrepancy cannot be ascertained. However, it is noted that instead of using pure fluid density values in the analysis or relying on estimated density values for the mutually saturated fluids, Shariat [32] performed independent density measurements on the mutually saturated fluids. As commented by Kashefi et al. [14], the deviation of these density values from the pure fluid density values seems to be unexpectedly large. However, that can probably not explain the anomalously high IFT values. The employed fluid density values could be expected to result in underestimated IFT – not overestimated. Inadequate system equilibration at the lower pressures would result in overestimated IFT, though, and could possibly explain the anomalously high values.

Table 3
Literature IFT data sets for methane/water system at 373 K (100 °C, 212°F) relevant for comparison with data in the present work. Range in pressure, p, is indicated.

Author(s)	p (MPa)	Comment	Note
Jennings and Newman [30]	10.1–60.8	Published 1971. Accepted for many years as the most consistent reference data set.	[1]
Wiegand [22]	10.0–260.0	Published 1993. Superior pressure range. The data fall above those of Jennings and Newman [30]. A selection of data points was published by Wiegand and Franck in 1994 [23].	[1]
Sachs and Meyn [3]	0.3–60.0	Published in 1995. The data fall close to those of Wiegand [22].	[2]
Tian et al. [31]	10.0–100.0	Published 1997. The data fall close to those of Wiegand [22].	[1]
Shariat [32]	7.3–133.0	Published 2014. The data fall significantly above those of Wiegand [22] at the lower pressures and below at higher pressures.	[3]
Kashefi et al. [14]	3.7–82.8	Published 2016. The data fall between those of Jennings and Newman [30] and Wiegand [22] and are in very good agreement with the data in the present work.	[1]

[1] Tabulated data.
[2] Regression line read from diagram stated to deviate less than 0.2% from experimental data points.
[3] Data points read from diagram.

The methane/water IFT data measured in this work at 448.45 K cannot as easily be compared directly with literature data. Only one data set of Jennings and Newman [30] at 350°F (449.8 K) is sufficiently close in temperature for direct comparison. Comparison shows that our data fall at approximately 5% higher value – just as at 373.15 K (Fig. 6). However, it is possible to compare the temperature dependence of the different data sets. Such comparison is revealing. Fig. 7 shows the temperature dependence at fixed pressure 60 MPa.

The comparison in Fig. 7 is made for pressure 60 MPa because that pressure falls within or close to the pressure range of all works referred to in Fig. 6 and because the pressure dependence is not very strong at that high pressure. Comparison of data sets for that pressure should therefore highlight systematic differences between the data sets. In Fig. 7, the data points of Wiegand [22] and Tian et al. [31] were taken directly from tabulated values. (A misprint is noted in Table 5 in the paper by Wiegand and Franck [23]. The tabulated IFT value at 298 K for 60 MPa reads 46.69 mN·m^{-1} but should according to the original work of Wiegand [22] read 49.69 mN·m^{-1}.) The data points of Sachs and Meyn [3] were read from reported regression lines. The data points of Shariat [32] were obtained by interpolation of plotted data points. All other data points, except the data point of Jennings and Newman [30] at 449.8 K, were obtained by interpolation of tabulated values. The data point of Jennings and Newman [30] at 449.8 K was found by a relatively small extrapolation in pressure of tabulated values.

Fig. 7 shows (like Fig. 6) that our data fall well within the range of previously published data. Here, the data sets of Shariat [32] and Jennings and Newman [30] represent the upper and lower bound to the range of the data, respectively. As noted, our data fall approximately 5% above those of Jennings and Newman [30]. Our data fall approximately 7% below those of Shariat [32]. Both differences appear to be significant. The relative combined standard uncertainty in our data is estimated to 0.7% (cf. Section 2.5). Jennings and Newman [30] indicate uncertainty of 1%, whereas Shariat [32] indicates uncertainty of 4–5%. At 60 MPa the temperature sensitivity coefficient ($\partial\gamma/\partial T$) of our data is approximately −0.13 mN·m^{-1}/K. The temperature sensitivity coefficient of the data sets of Shariat [32] and Jennings and Newman [30] agree with that value within 10%. As expected from Fig. 6, our data point at 373.15 K is within uncertainty equal to that of Kashefi et al. [14]. Extrapolation of our data to lower temperatures appears to be consistent with their data point at 311.0 K. However, their data do not agree as well with our data above 373.15 K. At higher temperatures the data of Kashefi et al. [14] fall close to those of Shariat [32]. However, considering that Kashefi et al. [14] reckon with approximately 6% uncertainty (combined expanded uncertainty) in their IFT values, the apparent difference between their data and our data at temperatures above 373.15 K may not be significant. Although the estimated uncertainty of the data of Kashefi et al. [14] is significantly larger than that of our data, it is noted that the temperature sensitivity coefficient determined by their two lower temperature data points at 311.0 K and 373.2 K is like that of our data set, and not much different from that determined by their two higher temperature data points at 423.2 K and 473.2 K.

The striking feature of Fig. 7 is that the IFT data of Wiegand [22] and those of Tian et al. [31], which follow the former closely (the deviation is smaller than 0.4%), deviate significantly from the linear dependence on temperature indicated by the other data sets. The data of Jennings and Newman [30] are clearly linear in temperature. The data of Shariat [32] and Kashefi et al. [14] exhibit larger scatter but within their stated uncertainty, indicate no significant deviation from linear trend. Considering the smaller stated uncertainty (0.3%) of the data of Sachs and Meyn [3], their data could indicate some deviation from linear trend, but barely so.

The absolute value of the temperature sensitivity coefficient of the data sets of Wiegand [22] and Tian et al. [31] below 373 K would seem to be 0.06 mN·m^{-1}/K, which is approximately a factor 2 smaller than

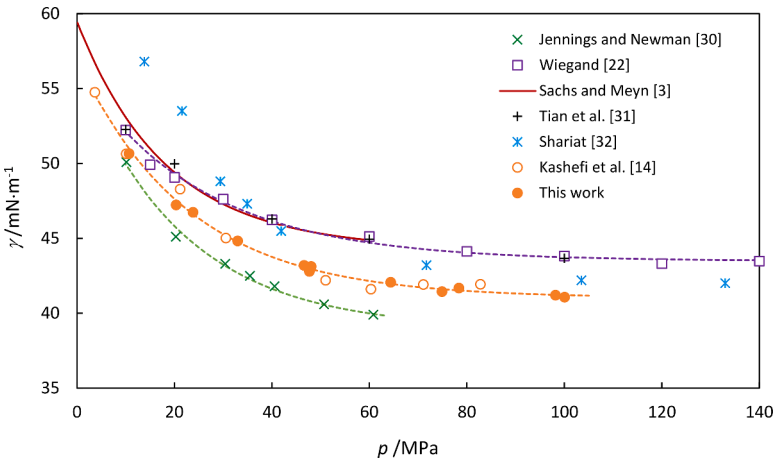

Fig. 6. Methane/water IFT, γ, at 373.15 K versus pressure, p, measured in this work compared with literature data sets (only part is shown of the data set of Wiegand [22], which extends to 260 MPa). Trend lines (broken lines) are shown for three data sets: those of Jennings and Newman [30], Wiegand [22], and Kashefi et al. [14]. The two former trendlines represent the lower and upper bound, respectively, to the range of the data at the higher pressures. The latter trendline is within uncertainty identical to that of this work. All trendlines are of the form given by Eq. (4). The data of Sachs and Meyn [3] are presented by their published regression line, which is stated to deviate from the measured data points by less than 0.2%.

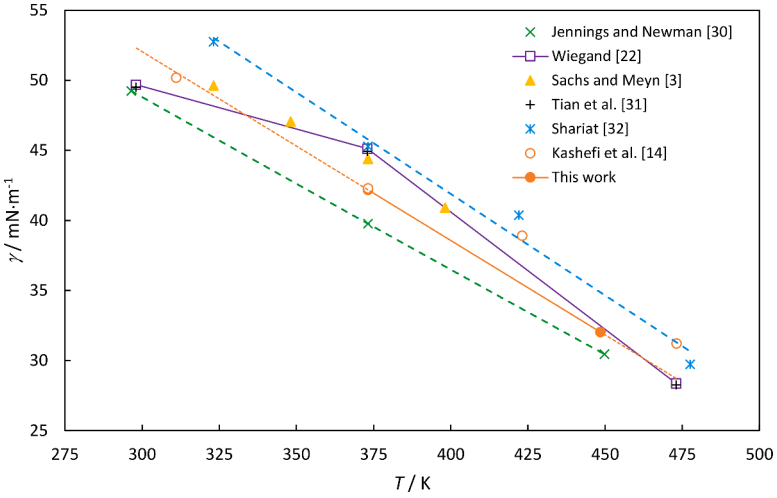

Fig. 7. Methane/water IFT at 60 MPa versus temperature, T, measured in this work compared with literature data. The line connecting the two data points of this work is extended to lower and higher temperatures for illustrative purpose (dotted line segments). The three data points of Wiegand [22] are connected for emphasise. Dashed green and blue lines represent the linear trendlines of the data of Jennings and Newman [30] and Shariat [32], respectively, which bound the data on the low and the high side.

that of the other data sets in Fig. 7 and nearly a factor 3 smaller than the absolute value of their sensitivity coefficient above 373 K. The average overall uncertainty of 1–2% estimated by Wiegand [22] and 1.5% estimated by Tian et al. [31] do not allow for the observed deviation from linear trend in their data. Although such deviation from linearity is unexpected, it is not discussed by the authors. Actually, Wiegand [22] explicitly assumes linearity with reference to the phenomenological Eötvös rule, i.e., that the IFT of most fluid systems exhibit approximate linear dependence on temperature, e.g. [35].

The close agreement between the data sets of Wiegand [22] and Tian et al. [31] would seem to rule out the possibility of a random error of analysis. It is noted that the data points of these workers at 298 K fall within the hydrate formation region and could for that reason be biased. To be sure, Wiegand [22] reports problems with hydrate formation for pressures higher than 42 MPa at 298 K. However, if so, also the data point of Jennings and Newman [30] at 74°F (296.5 K) could possibly be affected. But that does not seem to be the case. The data set of Jennings and Newman [30] is clearly linear. One could speculate whether the data points of Wiegand [22] and Tian et al. [31] at 373 K could be affected. That should not be possible, though. The data points at 373 K fall far outside the hydrate formation region. However, it is noted that hydrate dissolution is a complex process that has been discussed over many years and is still far from well understood, e.g. [36–41]. Could it be that hydrates formed at conditions within the stable hydrate region can subsist at or near the methane/water interface for some time after bringing the system out of the hydrate region? Anyway, the methane activity in the interface appears to be a decisive factor for the behaviour of the IFT between methane and water. That was indicated already by Wiegand and Franck [23] and has later been corroborated by many studies, e.g. [14,28,42]. Hydrate structures in the interface – or for that matter, adsorbed trace impurities – could therefore influence the behaviour of the IFT. It is perhaps indicative that the difference between the data sets in Fig. 7 seems to decrease with increasing temperature. It would have been interesting if the authors of the various works referred to had given more details on the IFT measurement procedure such as whether one and the same sample was used at all temperatures, whether the temperature was raised or lowered, whether the pressure was raised or lowered, and the duration of the measurement sequence. Unfortunately, few details are given. Jennings and Newman [30] and Sachs and Meyn [3,4] comment, though, that measurements at each temperature were taken in order of increasing pressure and then decreasing pressure without observing any hysteresis in IFT value.

The evidence of non-linear temperature dependence in the literature data sets can be strengthened by comparing results at a lower pressure, which allows more literature data to be included for comparison. Fig. 8 compares the data of the present work with literature data at 30 MPa. For clarity, Fig. 8a and Fig. 8b compare the data in this work with literature data exhibiting non-linear trend and linear trend, respectively. Fig. 8a includes in addition to data sets from the works referred to in Fig. 7, data sets of Ren et al. [43], Zhao et al. [44], and Liu et al. [1]. Fig. 8b includes the line connecting the three data points of Wiegand [22] for reference. The data points of Ren et al. [43] and Zhao et al. [44]

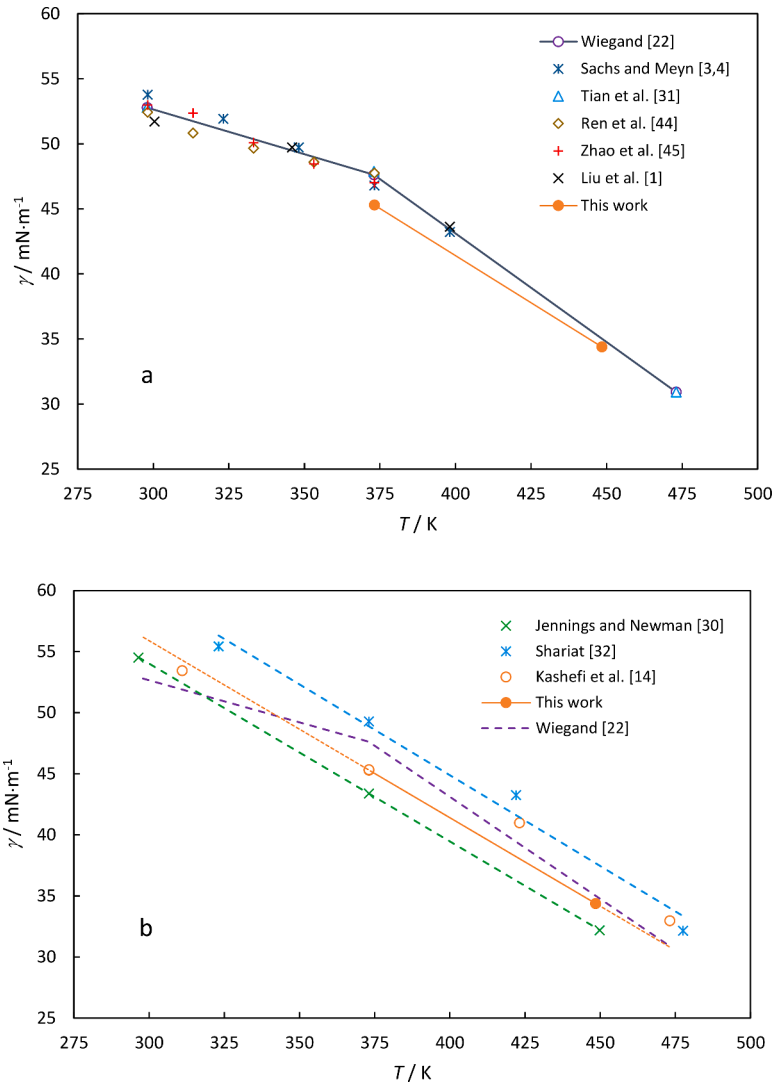

Fig. 8. Methane/water IFT at 30 MPa versus temperature, T, measured in this work compared with literature data sets exhibiting (a) non-linear trend and (b) linear trend. In (a) the data points of Wiegand [22] are connected by solid line. For comparison, a similar dashed line representing the data of Wiegand [22] is included in (b). In (b) the two data points in this work are connected by a solid line that is extrapolated to lower and higher temperatures (dotted line segments). Trend lines (dashed lines) are shown for the two data sets representing the upper and lower bound to the range of the data, i.e., those of Shariat [32] and Jennings and Newman [30], respectively.

were taken directly from tabulated values. The data points of Liu et al. [1] were found by interpolation of tabulated values.

Fig. 8 allows several interesting observations:

- The significant non-linearity of the data of Wiegand [22] and Tian et al. [31] (and possibly those of Sachs and Meyn [3]) at 60 MPa, observed in Fig. 7, is reproduced at the lower pressure of 30 MPa in Fig. 8a. (The three data points of Tian et al. [31] are not easily separated from those of Wiegand [22] because the deviation between the data sets is smaller than 0.5%.) As in Fig. 7, the absolute value of the temperature sensitivity coefficient of the data of Wiegand [22] and Tian et al. [31] below 373 K (0.07 mN·m^{-1}/K) is approximately a factor 2 smaller than that of our data (0.14 mN·m^{-1}/K). Because 30 MPa is below the hydrate formation pressure at 298 K, this would seem to make hydrate formation a less likely explanation for the observed non-linearity. However, as noted above, details of experimental procedure not reported in the works referred to, such as sequence of temperatures and pressures and duration of measurement series, could be relevant for this discussion.
- In Fig. 8a the IFT data points of Ren et al. [43] and Zhao et al. [44] fall close to the line connecting the two lower temperature data points of Wiegand [22] and thus provide independent confirmation of the data of Wiegand [22] and Tian et al. [31]. The temperature sensitivity coefficient of the data sets of Ren et al. [43] and Zhao et al. [44] agree within 15% with the data of Wiegand [22] and Tian et al. [31] below 373 K. Ren et al. [43] indicate that the maximum error in their reported IFT values is approximately 0.1%, which is close to the theoretical best performance level of the employed ADSA method. Considering that the stated uncertainty of the gas and water density values used in their analysis are considerably larger, it seems that the above maximum error value could be underestimated. Zhao et al. [44] indicate that the maximum error in their analysis should be smaller than 1%.
- Further, also the three data points of Liu et al. [1] fall close to the line connecting the data points of Wiegand [22]. However, considering their (conservatively) estimated uncertainty of 5%, the deviation from linearity may not be significant. It is of significance, though, that similar non-linearity is observed also in their IFT data for methane and brines with salinities of 1, 5, 10, and 20 wt% NaCl. This indicates that the non-linearity observed for methane/pure-water IFT in Fig. 8a is probably significant.
- The linear trend (within experimental uncertainty) observed in Fig. 7 for the data of Jennings and Newman [30], Shariat [32], and Kashefi et al. [14] at 60 MPa is reproduced at the lower pressure of 30 MPa in Fig. 8b. As in Fig. 7, the temperature sensitivity coefficient of the data sets of Jennings and Newman [30] and Shariat [32] agree within 10% with the value of our data.

There are a few more works that report IFT values for the methane/water system up to 30 MPa that are not included in Fig. 8. Villablanca-

Ahues et al. [45] have recently reported experimental IFT data for the three temperatures 298.15 K, 323.15 K, and 348.15 K. However, their data do not allow any firm conclusion as to whether they conform to the Eötwös rule. The temperature range is relatively restricted and the reported IFT at 323.15 K is not significantly different from that reported at the higher temperature 348.15 K, which does not seem convincing. At 30 MPa the reported IFT at 323.15 K is even lower than at the higher temperature. However, their data points at 298.15 K and 348.15 K agree with the corresponding data points of Sachs and Meyn [3,4] within 1%, which indicate a trend like that of the other data sets in Fig. 8a. Their data point at 323.15 K, which falls approximately 8% below the corresponding data point of Sachs and Meyn [3] would seem to be anomalous.

Other works report data for only one or two temperatures and hence, cannot clarify whether there is a linear or non-linear dependence on temperature. One data set of Sun et al. [46] (limited to one single temperature, 298.2 K) agrees with the data point of Wiegand [22] at 30 MPa (but deviates significantly at lower pressures). A data set published by Zain et al. [47] (two data points at 23 °C and 100 °C) is probably in agreement with the data of Jennings and Newman [30] in Fig 8b – and the linear dependence on temperature observed for that data set. However, the experimental uncertainty in the data of Zain et al. [47] seems to be relatively large (the authors do not give any estimate of uncertainty, but it is probably of the order of 10%).

Mention could also be made of the methane/water IFT data published by Khosharay and Varaminian [48] and Yasuda et al. [49]. Both report methane/water IFT data for five isotherms. However, these works address the low-temperature range and are restricted to pressures lower than the onset pressure of hydrate formation. The maximum temperature and pressure of the data of Khosharay and Varaminian [48] are 312.15 K and 6 MPa, respectively. The maximum temperature and pressure of the data of Yasuda et al. [49] are 298.15 K and 10 MPa, respectively. These two data sets are complementary to the data sets discussed above addressing the high-temperature and high-pressure range. It is therefore not possible to compare the data sets directly with the high-temperature data sets at 30 MPa in Fig. 8, but it is of interest that both data sets appear to agree with the Eötvös rule. Both data sets appear to depend linearly on temperature at constant pressure, but this observation should be considered tentative because of the limited range of temperatures investigated. Both works report data for the 298.15 K isotherm that are in excellent agreement up to 6 MPa. Their data at 298.15 K can also be compared directly with some other literature data sets. They are in good agreement with the corresponding data set of Sachs and Meyn [4] (up to 6 MPa) and the older data sets of Massoudi and King, Jr. [50] and Jho et al. [51]. All these data sets extrapolate (within uncertainty) in the low-pressure limit to the recommended surface tension value of pure water, as they should. In fact, that is the case for all works discussed above that report data at or near the 298 K isotherm, except for the works of Ren et al. [43] and Sun et al. [46]. These data sets extrapolate to significantly higher value than the surface tension of water. That is the case also for a 74°F data set of Hough et al. [33], which unlike their data at elevated temperatures is probably not biased by impurities (see discussion above). Extrapolation to higher IFT value than the surface tension of water could possibly be explained by inaccurate magnification factor of the drop shape analysis. It is noted that Tian et al. [31] report an IFT value at 298 K and atmospheric pressure that is significantly lower than the surface tension of water. That can probably be explained by an anomalous atmospheric pressure measurement. The 25 °C data reported by Slowinski et al. [52] extrapolates to IFT value lower than the water surface tension value, but that data set was obtained by the capillary rise method and the deviation can probably be explained by some other method specific inaccuracy of the analysis. Also the older data set by Hocott [53] was obtained by the capillary rise method, but that data set deviates considerably from the other data sets discussed above – probably partly because it was not obtained with pure methane, but with a methane-rich hydrocarbon gas mixture.

However, it is interesting to note that although the data sets of Khosharay and Varaminian [48] and Yasuda et al. [49] are in good agreement for the 298.15 K isotherm, the temperature sensitivity coefficient of the data sets appears to differ significantly. The temperature sensitivity coefficient of the data of Khosharay and Varaminian [48] is approximately -0.15 mN·m^{-1}/K, which is like the sensitivity coefficients of the data sets in Fig. 8b. The typical temperature sensitivity of the data of Yasuda et al. [49] appears to be significantly smaller – the temperature sensitivity coefficient appears to fall in the range $-(0.08–0.10)$ mN·m^{-1}/K, and hence closer to the sensitivity coefficients of the data below 373 K in Fig. 8a. It is noted that the temperature dependence of the data of Yasuda et al. [49] appears to be like that of the older data set of Jho et al. [51].

It is finally noted that Lepski [54] reported methane/water IFT data for six isotherms in the range (52.5–126.8) °C for pressures up to 3500 psia. (A subset of the data was published by Lepski et al. [55]). In the literature, this data set has sometimes erroneously been referred to as a methane/pure-water IFT data set whereas the water phase used was a 5 wt% NaCl brine. The data set is therefore not directly relevant for our discussion. However, it is of interest that the data display linear dependence on temperature and yield a typical temperature sensitivity coefficient in the range $-(0.10–0.12)$ mN·m^{-1}/K. This result agrees with the more recent result obtained by Kashefi et al. [14] for a similar system of methane and 5 wt% NaCl-brine, except that the IFT values obtained by Kashefi et al. [14] fall 5–10% below those of Lepski [54].

In summary, there are surprisingly large variations between literature data sets for the methane/water IFT. The indications are that much of the variation can be explained by uncertainty of the different analyses arising both from random and systematic effects. However, after considering conventional sources of uncertainty, there seems to remain a certain systematic difference between published data sets that is difficult to explain. Why is it that a seemingly reproducible non-linear temperature dependence turns up in several independent literature data sets that cover a wide range of temperatures and not in others? Why is it that some literature data sets of more restricted temperature range appear to fall in line with those displaying non-linear temperature dependence and some do not? It is also surprising that despite recent improvements in IFT analysis technique, one of the older data sets – that of Jennings and Newman [30] – after 50 years still appears to be one of the more consistent. However, it is noted that Schmidt et al. [5] in their modelling work omitted part of the data of Jennings and Newman [30], stating that they "appeared to exhibit a strong discrepancy with the rest of the data set and the results obtained from the model". It appears that Schmidt et al. [5] were led to that conclusion (partly) by the discrepancy between the data of Jennings and Newman [30] and those of Ren et al. [43]. The data of Ren et al. [43] have been used for reference also in more recent modelling works, e.g. Zhang et al. [34], Niño-Amézquita and Enders [7], Pereira et al. [11], Villablanca-Ahues et al. [45]. However, with reference to Fig. 7 and Fig. 8, it appears still to be a matter of argument which data sets are the more representative – those showing non-linear dependence on temperature or those showing linear dependence.

5. Conclusion

In this work we have drawn attention to a peculiar inconsistency in the literature IFT data for the methane/water system. We have shown that there is close agreement between the data of Wiegand [22], Tian et al. [31], Ren et al. [43], Zhao et al. [44], Liu et al. [1] (and possibly those of Sachs and Meyn [3,4]). However, the trend of IFT versus temperature for these data sets seems to deviate from the linear trend of the data of Jennings and Newman [30], Shariat [32], and Kashefi et al. [14]. Our data seem to agree with the linear trend of the latter data sets. This inconsistency is both puzzling and disconcerting. Experimental data on methane/water IFT are currently used as reference data in many modelling works. It is therefore a matter of interest which data sets are

the more representative. The present work cannot provide conclusive evidence for or against a non-linear temperature dependence of the IFT for the methane/water system. However, it would seem to require more evidence than presented hitherto to accept deviation from the Eötvös rule. According to the molecular dynamics simulations of Mirzsaeifard et al. [56,57] such deviation is not to be expected.

CRediT authorship contribution statement

Bård J.A. Bjørkvik: Conceptualization, Methodology, Validation, Investigation, Resources, Writing – original draft, Writing – review & editing, Visualization, Supervision, Project administration.

Declaration of Competing Interest

The authors declare that they have no known competing financial interests or personal relationships that could have appeared to influence the work reported in this paper.

Data availability

Data will be made available on request.

Acknowledgement

The author would like to acknowledge permission by AkerBP ASA to publish the methane/water IFT data.

Supplementary materials

Supplementary material associated with this article can be found, in the online version, at doi:10.1016/j.fluid.2023.113834.

References

[1] Y. Liu, H.A. Li, R. Okuno, Measurements and modeling of interfacial tension for CO_2/CH_4/brine systems under reservoir conditions, Ind. Eng. Chem. Res. 55 (2016) 12358–12375, https://doi.org/10.1021/acs.iecr.6b02446.
[2] A. Firoozabadi, H.J. Ramey Jr., Surface tension of water-hydrocarbon systems at reservoir conditions, J. Can. Pet. Technol. 27 (1988) 41–48, https://doi.org/10.2118/88-03-03.
[3] W. Sachs, V. Meyn, Oberflächenspannung im System Methan/Wasser, Ein kurzer Blick auf Numerik und Genauigkeit der experimentellen Methode "Pendent-drop" sowie präzise experimentelle Resultate im Vergleich zur Literatur, Erdöle Erdgas Kohle 111 (1995) 119–121.
[4] W. Sachs, V. Meyn, Pressure and temperature dependence of the surface tension in the system natural gas/water: principles of investigation and the first precise experimental data for pure methane/water at 25°C up to 46.8MPa, Colloids Surf. A 94 (1995) 291–301, https://doi.org/10.1016/0927-7757(94)03008-1.
[5] K.A.G. Schmidt, G.K. Folas, B. Kvamme, Calculation of the interfacial tension of the methane-water system with the linear gradient theory, Fluid Phase Equilib. 261 (2007) 230–237, https://doi.org/10.1016/j.fluid.2007.07.045.
[6] R.P. Sutton, An improved model for water-hydrocarbon surface tension at reservoir conditions, in: Paper SPE-124968-MS presented at The 2009 SPE Annual Technical Conference and Exhibition, New Orleans, Louisiana, USA, October 4-7, 2009, https://doi.org/10.2118/124968-MS.
[7] O.G. Niño-Amézquita, S. Enders, Phase equilibrium and interfacial properties of water + methane mixtures, Fluid Phase Equilib. 407 (2016) 143–151, https://doi.org/10.1016/j.fluid.2015.05.005.
[8] W. Li, Z. Jin, Molecular dynamics simulations of natural gas-water interfacial tensions over wide range of pressures, Fuel 236 (2019) 480–492, https://doi.org/10.1016/j.fuel.2018.09.040.
[9] H. Mehrjoo, M. Riazi, M.N. Amar, A. Hemmati-Sarapardeh, Modeling interfacial tension of methane-brine systems at high pressure and high salinity conditions, J. Taiwan Inst. Chem. Eng. 114 (2020) 125–141, https://doi.org/10.1016/j.jtice.2020.09.014.
[10] Q. Guo, W. Hu, Y. Zhang, K. Zhang, B. Dong, Y. Qin, W. Li, Molecular dynamics simulation of the interfacial properties of methane-water and methane-brine systems, Mol. Simul. (2021), https://doi.org/10.1080/08927022.2021.1929969.
[11] A. da Silva Pereira, A.R.C. de Oliveira, P.F.G. Silvino, M. Bastos-Neto, S.M. P. Lucena, Neural network protocol to predict interfacial tension for CO_2/CH_4/Water-Brine ternary systems under reservoir temperature and pressure ranges, Pet. Sci. Technol. 40 (2022) 181–200, https://doi.org/10.1080/10916466.2021.1991375.
[12] S.M.I. Saad, A.W. Neumann, Axisymmetric drop shape analysis (ADSA): an outline, Adv. Colloid Interface Sci. 238 (2016) 62–87, https://doi.org/10.1016/j.cis.2016.11.001.
[13] J.W. Jennings Jr., N.R. Pallas, An efficient method for the determination of interfacial tensions from drop profiles, Langmuir 4 (1988) 959–967, https://doi.org/10.1021/la00082a030.
[14] K. Kashefi, L.M.C. Pereira, A. Chapoy, R. Burgass, B. Tohidi, Measurement and modelling of interfacial tension in methane/water and methane/brine systems at reservoir conditions, Fluid Phase Equilib. 409 (2016) 301–311, https://doi.org/10.1016/j.fluid.2015.09.050.
[15] S.M.I. Saad, Z. Policova, E.J. Acosta, A.W. Neumann, Range of validity of drop shape techniques for surface tension measurement, Langmuir 26 (2010) 14004–14013, https://doi.org/10.1021/la1020675.
[16] J.D. Berry, M.J. Neeson, R.R. Dagastine, D.Y.C. Chan, R.F. Tabor, Measurement of surface and interfacial tension using pendant drop tensiometry, J. Colloid Interface Sci. 454 (2015) 226–237, https://doi.org/10.1016/j.jcis.2015.05.012.
[17] J. Yang, K. Yu, Y.Y. Zuo, Accuracy of axisymmetric drop shape analysis in determining surface and interfacial tensions, Langmuir 33 (2017) 8914–8923, https://doi.org/10.1021/acs.langmuir.7b01778.
[18] Release R1-76 (2014) by The International Association for the Properties of Water and Steam (IAPWS), Revised Release on the Surface Tension of Ordinary Water Substance (June 2014). http://www.iapws.org/.
[19] E.W. Lemmon, M.L. Huber, M.O. McLinden, NIST Standard Reference Database 23, Reference Fluid Thermodynamic and Transport Properties – REFPROP, Version 9.1, National Institute of Standards and Technology, Gaithersburg MD 20899, USA, 2013.
[20] B.N. Taylor, C.E. Kuyatt, Guidelines for Evaluating and Expressing the Uncertainty of NIST Measurement Results, NIST Technical Note 1297, 1994 Edition. https://www.nist.gov/pml/nist-technical-note-1297.
[21] H.B. Callen, Thermodynamics and an Introduction to Thermostatistics, 2nd ed., John Wiley & Sons, New York, 1985.
[22] G. Wiegand, Messung der Grenzenflächenspannung binärer wäßriger Systeme bei hohen Drücken und Temperaturen (Dissertation), Universität Karlsruhe, Karlsruhe, 1993.
[23] G. Wiegand, E.U. Franck, Interfacial tension between water and non-polar fluids up to 473K and 2800bar, Ber. Bunseges. Phys. Chem. 98 (1994) 809–817, https://doi.org/10.1002/bbpc.19940980608.
[24] W.D. McCain Jr., J.P. Spivey, C.P. Lenn, Petroleum Reservoir Fluid Property Correlations, PennWell, Tulsa, 2011.
[25] M. Yarrison, K.R. Cox, W.G. Chapman, Measurement and modeling of the solubility of water in supercritical methane and ethane from 310 to 477K and pressures from 3.4 to 110MPa, Ind. Eng. Chem. Res. 45 (2006) 6770–6777, https://doi.org/10.1021/ie0513752.
[26] A. Hebach, G. Martin, A. Kögel, N. Dahmen, Interfacial Tension during Mass Transfer of CO_2 into Water in a Water-Saturated CO_2 Atmosphere at 298K and 6.6MPa, J. Chem. Eng. Data 50 (2005) 403–411, https://doi.org/10.1021/je049773j.
[27] Z. Wang, H. Tu, P. Guo, F. Zeng, T. Sang, Z. Wang, Fluid behavior of gas condendate system with water vapor, Fluid Phase Equilib. 438 (2017) 67–75, https://doi.org/10.1016/j.fluid.2017.01.018.
[28] C. Miqueu, J.M. Míguez, M.M. Piñeiro, T. Lafitte, B. Mendiboure, Simultaneous application of the gradient theory and Monte Carlo molecular simulation for the investigation of methane/water interfacial properties, J. Phys. Chem. B 115 (2011) 9618–9625, https://doi.org/10.1021/jp202276k.
[29] Y. Yang, A.K.N. Nair, S. Sun, Molecular dynamics simulation study of carbon dioxide, methane and their mixture in the presence of brine, J. Phys. Chem. B 121 (2017) 9688–9698, https://doi.org/10.1021/acs.jpcb.7b08118.
[30] H.Y. Jennings Jr., G.H. Newman, The effect of temperature and pressure on the interfacial tension of water against methane-normal decane mixtures, SPE J 11 (1971) 171–175, https://doi.org/10.2118/3071-PA.
[31] Y. Tian, Y. Xiao, H. Zhu, X. Dong, X. Ren, F. Zhang, Interfacial tensions between water and non-polar fluids at high pressures and high temperatures (Chinese), Acta Phys.-Chim. Sin. 13 (1997) 89–95, https://doi.org/10.3866/pku.Whxb19970120.
[32] A. Shariat, Measurement and Modeling Gas-Water Interfacial Tension at High Pressure/ High Temperature Conditions (Ph.D. Thesis), University of Calgary, Calgary, 2014.
[33] E.W. Hough, M.J. Rzasa, B.B. Wood, Interfacial tensions at reservoir pressures and temperatures; Apparatus and the water-methane system, Petroleum Transactions, AIME, 192 (1951) 57-60, J. Pet. Technol. 3 (1951) 57–60, https://doi.org/10.2118/951057-G.
[34] J. Zhang, Q. Feng, X. Zhang, X. Zhang, N. Yuan, S. Wen, S. Wang, A. Zhang, The use of an artificial neural network to estimate natural gas/water interfacial tension, Fuel 157 (2015) 28–36, https://doi.org/10.1016/j.fuel.2015.04.057.
[35] J. Lyklema, Fundamentals of Interface and Colloid Science, Vol. III, Liquid-Fluid Interfaces, Academic Press, San Diego, 2000.
[36] S. Takeya, A. Hori, T. Hondoh, T. Uchida, Freezing-memory effect of water on nucleation of CO_2 hydrate crystals, J. Phys. Chem. B 104 (2000) 4164–4168, https://doi.org/10.1021/jp993759+.
[37] L.A. Stern, S. Circone, S.H. Kirby, W.B. Durham, Temperature, pressure, and compositional effects on anomalous or "self" preservation of gas hydrates, Can. J. Phys. 81 (2003) 271–283, https://doi.org/10.1139/p03-018.
[38] S.A. Bagherzadeh, S. Alavi, J. Ripmeester, P. Englezos, Formation of methane nano-bubbles during hydrate decomposition and their effect on hydrate growth, J. Chem. Phys. 142 (2015), 214701, https://doi.org/10.1063/1.4920971.

[39] T. Uchida, K. Yamazaki, K. Gohara, Generation of micro- and nano-bubbles in water by dissociation of gas hydrates, Korean J. Chem. Eng. 35 (2016) 1749–1755, https://doi.org/10.1007/s11814-016-0032-7.
[40] Z.-D. Li, X. Tian, Z. Li, J.-Z. Xu, H.-X. Zhang, B.-C. Gan, L. Li, Experimental study on influences of self-preservation effects and memory effects on the hydrate decomposition process, Lithosphere (12) (2022), 7780662, https://doi.org/10.2113/2022/7780662. Special Issue.
[41] A. Hassanpouryouzband, E. Joonaki, M.V. Farahani, S. Takeya, C. Ruppel, J. Yang, N.J. English, J.M. Schicks, K. Edlmann, H. Mehrabian, Z.M. Aman, B. Tohidi, Gas hydrates in sustainable chemistry, Chem. Soc. Rev. 49 (2020) 5225–5309, https://doi.org/10.1039/C8CS00989A.
[42] A. Ghoufi, P. Malfreyt, Numerical evidence of the formation of a thin microscopic film of methane at the water surface: a free energy calculation, Phys. Chem. Chem. Phys. 12 (2010) 5203–5205, https://doi.org/10.1039/B924886B.
[43] Q.-Y. Ren, G.-J. Chen, W. Yan, T.-M. Guo, Interfacial tension of (CO_2 + CH_4) + water from 298 K to 373 K and pressures up to 30 MPa, J. Chem. Eng. Data 45 (2000) 610–612, https://doi.org/10.1021/je990301s.
[44] G.-Y. Zhao, W. Yan, G.-J. Chen, X.-Q. Guo, Measurement and calculation of high-pressure interfacial tension of methane + nitrogen/water system (Chinese), Shiyou Daxue Xuebao, Ziran Kexueban /J. Univ. Pet., China, Ed, Nat. Sci. 26 (2002) 75–78, 82.
[45] R. Villablanca-Ahues, R. Nagl, T. Zeiner, P. Jaeger, Interfacial tension and phase equilibria for binary systems containing (CH_4-CO_2)+(n-dodecane; n-butanol; water), Fluid Phase Equilib. 570 (2023), 113783, https://doi.org/10.1016/j.fluid.2023.113783.
[46] C.-Y. Sun, G.-J. Chen, L.-Y. Yang, Interfacial tension of methane + water with surfactant near the hydrate formation conditions, J. Chem. Eng. Data 49 (2004) 1023–1025, https://doi.org/10.1021/je049948p.
[47] Z.M. Zain, N. Ahmad, D.M.A. Raja, M.E. Daud, P. Sigmund, Interfacial tension measurements on oil/gas/water systems using state-of-the-art vapour-liquid equilibrium interfacial tension (VLE-IT) equipment, in: Paper OSEA 96074 presented at The 11th Offshore South East Asia Conference, Singapore, 24-27 September, 1996.
[48] S. Khosharay, F. Varaminian, Experimental and modelling investigation on surface tension and surface properties of (CH_4 + H_2O), (C_2H_6 + H_2O), (CO_2 + H_2O) and (C_3H_8 + H_2O) from 284.15 K to 312.15 K and pressures up to 60 bar, Int. J. Refrig. 47 (2014) 26–35, https://doi.org/10.1016/j.ijrefrig.2014.08.003.
[49] K. Yasuda, Y.H. Mori, R. Ohmura, Interfacial tension measurements in water–methane system at temperatures from 278.15 K to 298.15 K and pressures up to 10 MPa, Fluid Phase Equilib. 413 (2016) 170–175, https://doi.org/10.1016/j.fluid.2015.10.006.
[50] R. Massoudi, A.D. King Jr., Effect of pressure on the surface tension of water. Adsorption of low molecular weight gases on water at 25.deg, J. Phys. Chem. 78 (1974) 2262–2266, https://doi.org/10.1021/j100615a017.
[51] C. Jho, D. Nealon, S. Shogbola, A.D. King Jr., Effect of pressure on the surface tension of water: adsorption of hydrocarbon gases and carbon dioxide on water at temperatures between 0 and 50°C, J. Colloid Interface Sci. 65 (1978) 141–154, https://doi.org/10.1016/0021-9797(78)90266-7.
[52] E.J. Slowinski Jr., E.E. Gates, C.E. Waring, The effect of pressure on the surface tensions of liquids, J. Phys. Chem. 61 (1957) 808–810, https://doi.org/10.1021/j150552a028.
[53] C.R. Hocott, Interfacial tension between water and oil under reservoir conditions, Trans. AIME 132 (1938) 184–190, https://doi.org/10.2118/939184-G.
[54] B. Lepski, Gravity-Assisted Tertiary Gas Injection Process in Water-Drive Oil Reservoirs (Ph.D. Thesis), LSU Historical Dissertations and Theses 6498, Louisiana State University and Agricultural and Mechanical College, Louisiana, 1997.
[55] B. Lepski, Z. Bassiouni, J.M. Wolcott, Screening of Oil Reservoirs for Gravity Assisted Gas Injection, in: Paper SPE-39659-MS presented at the SPE/DOE Improved Oil Recovery Symposium in Tulsa, Oklahoma, April 19–22, 1998, https://doi.org/10.2118/39659-MS.
[56] S. Mirzaeifard, P. Servio, A.D. Rey, Molecular dynamics characterization of temperature and pressure effects on the water-methane interface, Colloid Interface Sci. Commun. 24 (2018) 75–81, https://doi.org/10.1016/j.colcom.2018.04.004.
[57] S. Mirzaeifard, P. Servio, A.D. Rey, Molecular dynamics characterization of the water-methane, ethane, and propane gas mixture interfaces, Chem. Eng. Sci. 208 (2019), 114769, https://doi.org/10.1016/j.ces.2019.01.051.